ISSN 1063-7788, Physics of Atomic Nuclei, 2019, Vol. 82, No. 11, pp. 1494–1498. © Pleiades Publishing, Ltd., 2019.
Russian Text © The Author(s), 2019, published in Yadernaya Fizika i Inzhiniring, 2019, Vol. 10, No. 2.

ENGINEERING DESIGN OF NUCLEAR PHYSICS EQUIPMENT

Magnetic Drag and Energy Losses in Noncontact Bearings Based on Superconducting Tapes

A. I. Podlivaev[a],*, I. A. Rudnev[a], and I. V. Anischenko[a]

[a] *Department of Condensed Matter and Nanosystems, National Research Nuclear University MEPhI (Moscow Engineering Physics Institute), Moscow, 115409 Russia*

**e-mail: mephizic@gmail.com*

Received June 28, 2019; revised July 8, 2019; accepted July 8, 2019

Abstract—In the paper, the problem of magnetic drag and origination of energy losses in noncontact bearings based on high-temperature superconducting tapes is considered. The model configurations of bearings in which a superconducting tape is a stator and a set of permanent magnets is a rotor are investigated. It is shown that the magnetic friction can be neglected in the case where more than eight permanent magnets compose the rotor. This result indicates the possibility to create scaled magnetic bearings for the systems of long-term energy storage, for example, flywheel energy storage systems.

Keywords: HTS, magnetic friction, magnetic drag

DOI: 10.1134/S1063778819110164

INTRODUCTION

The application of superconductor/permanent magnet pairs in noncontact bearings is quite promising. The absence of friction, due to the lack of direct mechanical contact between their moving parts, provides the efficient use of magnetic bearings in high-speed rotating machinery: flywheel energy storage systems, gyroscopes, and similar devices (see, for example [1]).

Manufacturing a superconducting rotor (stator) made of a three-dimensional high-temperature superconductor (HTS) is a challenging technological problem due to the brittleness of the material and the complexity of the annealing regime aimed at providing the homogeneity of its properties. A multilayer superconductor composed of stacked HTS tapes can be an alternative to the 3D superconductor [2]. Short-circuit coils made of HTS can be considered the analog of a stack of tapes [3]. HTS tapes have certain advantages as compared to 3D materials. The technology of making superconducting composites of arbitrary form consisting of tapes is simpler. The superconducting characteristics of a stack of tapes are as good as those of a 3D material [4]. In addition, the HTS tapes possess higher mechanical properties than 3D materials.

The magnetic rotor manufacturing is also a complex technological problem. A single-piece magnet with the required form and dimensions has to maintain an axially symmetric magnetic field. A composed magnet can be an alternative to the single-piece magnet (as in the case with a superconductor). The composed magnet is a mosaic consisting of a great number of small magnets. Each element of the mosaic is a homogeneously magnetized ferromagnet in the form of rectangular parallelepiped. A disadvantage of this mosaic is the magnetic field inhomogeneity, most significant at the interface between neighboring elements and able to induce a hysteresis magnetic reversal in the superconductor, which is accompanied by energy dissipation (see, for example, [5]) and, therefore, emergence of friction force in the bearing. This paper is focused on the theoretical investigation of the influence of the inhomogeneity of the magnetic field of a composed magnet on the friction force in a bearing whose superconducting stator is formed by single-layer or multilayer rings made of second-generation HTS tapes.

DESCRIPTION OF THE BEARING MODEL. GEOMETRY. BASIC EQUATIONS

The bearing studied by us consists of a rotor and a stator. The division into the "rotor" and "stator" is conventional. The inner shaft of the bearing can rotate with the exterior part fixed, and the exterior part can rotate around the fixed inner axis. To be definite, we assume hereinafter that the superconducting part of the bearing is the fixed stator, and the rotor is a set of permanent magnets of small sizes. This choice is mainly stipulated by the fact that the fixed superconductor cooling to avoid thermodynamic instability is technically simpler [6, 7]. In Figs. 1 and 2, the bearings with square and octagonal rotors, respectively, are presented. Below, the number of magnets in a rotor is

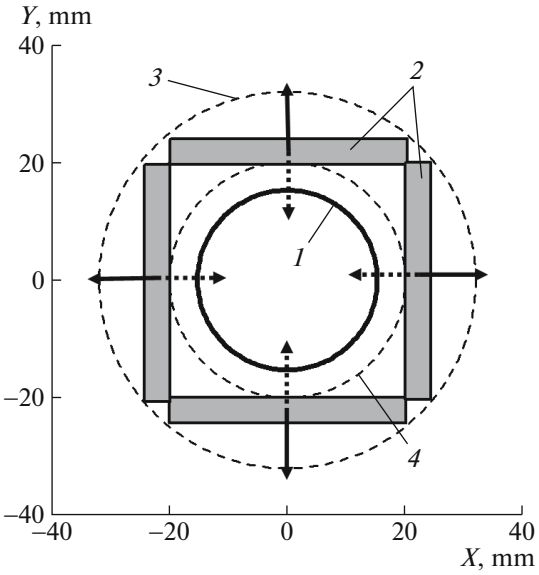

Fig. 1. Bearing with a square magnetic rotor: (*1*) superconducting stator; (*2*) magnetic rotor; (*3*) outer boundary and (*4*) inner boundary of the magnetic rotor (at its rotation). Solid and dotted arrows on the magnets specify the direction of magnetization of the neighboring magnet (along the *Z* axis).

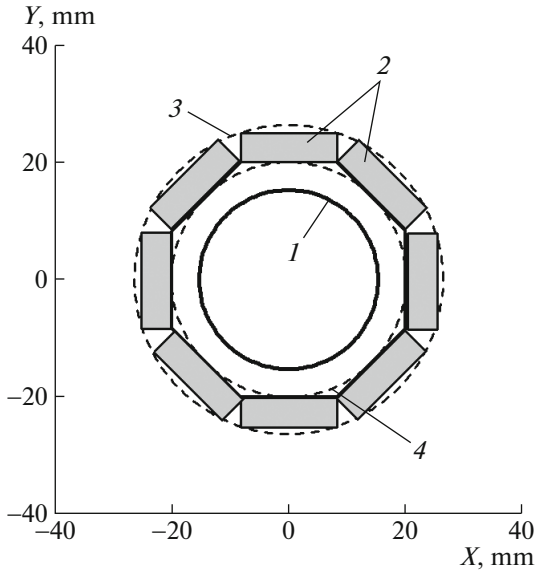

Fig. 2. Bearing with an octagonal magnetic rotor: (*1*) superconducting stator; (*2*) magnetic rotor; (*3*) outer boundary and (*4*) inner boundary of the magnetic rotor (at its rotation).

denoted as N_{mag} ($N_{\text{mag}} = 4, 8, 16$). The following sizes of the magnetic rotor are chosen for calculations. The inner boundary of each rotor has the radius of 20 mm (the inner circle is shown by dashed line in Figs. 1 and 2). The outer radii are 32.016 mm and 26.34 mm for the square and octagonal rotors, respectively (the outer circle shown by dashed line in Figs. 1 and 2). The magnet is 5 mm in thickness for each rotor, and the width of the magnet dZ is 12 mm along the Z axis. When selecting the parameters of the tape, we considered the 12 mm SuperOx tape that was promising for many technical applications (for example, for current limiters [8]). If we denote the magnetic moment density vector as $\mathbf{m}(\mathbf{r}')$ at the point of space with the radius vector $\mathbf{r}'$, then the magnetic field induction vector created by the magnet (with the volume V) at the point $\mathbf{r}'$ can be written in the following form [9]:

$$\mathbf{B}(\mathbf{r}) = \mu_0 \int_V \left[\frac{3\mathbf{n}(\mathbf{n}, \mathbf{m}(\mathbf{r}')) - \mathbf{m}(\mathbf{r}')}{|\mathbf{r} - \mathbf{r}'|^3} \right] d^3 r', \quad (1)$$
$$\mathbf{n} = (\mathbf{r} - \mathbf{r}')/|\mathbf{r} - \mathbf{r}'|.$$

The modulus of vector $\mathbf{m}(\mathbf{r}')$ was chosen so that the value of the magnetic field induction of an individual magnet (Fig. 1) at the center of its surface was 0.3 T.

Usually, the thickness of HTS tape is ~0.1 mm; therefore, in this paper, as in [4], we assume the thickness of the stator winding to be zero. We assume the critical current density in a solid single-layer HTS ring to be j_c and in a double-layer ring to be $2j_c$. The critical current density on the boundaries of neighboring rings that are perpendicular to the Z axis is zero. The Z coordinates of the stator ring boundaries coincide with the boundaries of the rotor heteropolar magnets. These boundary coordinates are $Z = 0$, $\pm dZ/2$, $\pm 2dZ/2$, $\pm 3dZ/2$, etc.

When the number of magnets in the rotor is large ($N_{\text{mag}} \gg 1$) and the HTS ring width is small in comparison with their perimeter ($d_p/d_Z \gg 1$), the stator curvature can be neglected, and the superconducting current density identification problem formulated in cylindrical coordinates (ρ, φ, Z), where $\rho = R_S$, can be replaced by the two-dimensional problem set in the plane (p, Z) with $p = R_S\varphi$. In this case, the rectangle $-d_Z/2 \le Z \le d_Z/2$, $-d_p/2 \le p \le d_p/2$ is the domain of definition of the magnetic field and the current densities. The boundary conditions are periodic both over the angular variable p and over the variable Z (it is assumed that the rotor consists of an infinite number of adjacent heteropolar ring magnets). The replacement of the cylindrical problem with the planar one is substantiated by the considerations that, firstly, the ratio $d_p/d_Z = 8$ is sufficiently large and, secondly, rotors with a larger number of magnets are of greater interest ($N_{\text{mag}} = 8$ and 16). We consider the square rotor for the qualitative determination of the bearing friction dependence on the number of magnets. In addition, the influence of the external field inhomogeneity (over the angular variable) on the superconducting current distribution is manifested the most in the square rotor.

The external magnetic field of the magnetic rotor in the stator was calculated by formula (1). The magnetic field induction component normal to the surface of

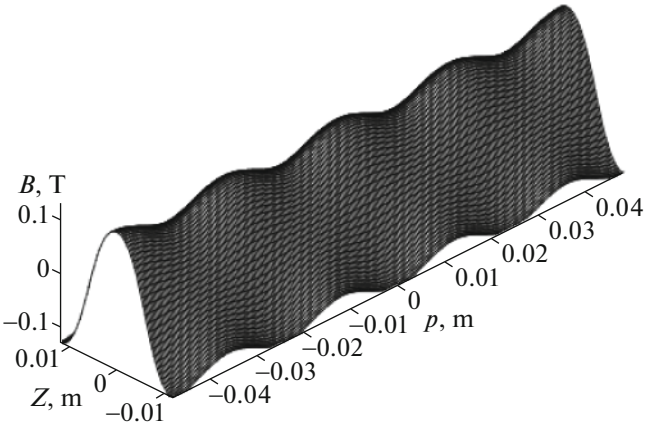

Fig. 3. Normal component of the magnetic field induction B_ρ on the developed surface of the stator.

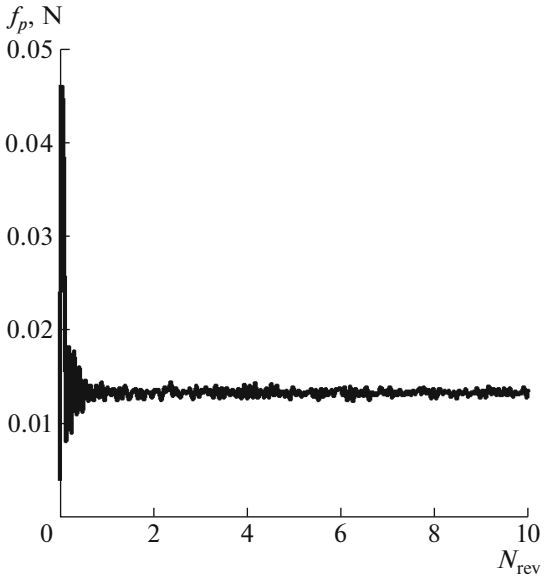

Fig. 4. Friction force as a function of the number of revolutions of the square rotor.

the stator on the square rotor surface is presented in Fig. 3. The variation of the magnetic field amplitude $(B_{max} - B_{min})/(B_{max} + B_{min})$ when the coordinate $Z = 0$ is 14.8%, 1.3%, and 0.2% for $N_{mag} = 4$, 8, and 16, respectively. The idea of applying the inhomogeneous (periodic) external magnetic field is not new. Hence, in [10, 11], a set of magnets of different polarities was used to create a periodic configuration; however, the main feature of the present paper is the calculation of the HTS tape in a weakly varying field, which acts on the superconductor during an unlimited number of periods. We describe the field dependence of the critical current of the superconducting tape within the double-exponential model [12], in which the density of the surface currents $j_c(B)$ of the HTS tape can be written in the following form:

$$j_c(B) = A_1 \exp(-|B|/\beta_1) + A_2 \exp(-|B|/\beta_2), \qquad (2)$$

with the parameters $A_1 = 12.9$ kA/m, $A_2 = 13.8$ kA/m, $\beta_1 = 0.08$ T, and $\beta_2 = 1.92$ T. The spatial grid step in the presented calculations was $\delta h \sim 0.375$ mm. The calculations were performed within the simulation of the superconductor critical state initially proposed in [13], whose modifications and applications are given in [4]. The detailed description of the mathematical problem and algorithm of the numerical calculation for the case of field dependence (2) are presented in [4, 14]; they are not given in the present paper in view of their cumbersomeness.

At the first stage, the external magnetic field proportional to the rotor field without the rotor rotation increased monotonically from zero to the value determined by expression (1). Further, the rotor was rotated by 40 revolutions (hereinafter, the number of revolutions is denoted as N_{rot}). The corresponding density of superconducting currents was detected. In the plane problem, one revolution of the cylindrical configuration corresponds to a shift of the magnetic field over the variable p by the period d_p. In this case, the tangential component of the force of interaction of the rotor field B_ρ with the stator currents (friction force) f_p for a ring of the stator is determined by the Ampere law:

$$f_p = \int_{-d_p/2}^{d_p/2} dp \int_{-d_Z/2}^{d_Z/2} B_\rho(p,Z) j_Z(p,Z) dZ. \qquad (3)$$

RESULTS AND DISCUSSION

The dependence of the friction force in the square stator ($N_{mag} = 4$) on the number of rotor revolutions is presented in Fig. 4, where it is shown that the friction force is set within one revolution. For rotors with a larger number of magnets ($N_{mag} = 8$ and 16), the friction force is set in less than two revolutions. Since we do not consider the character of transients in this paper, the friction force is determined by averaging this parameter over the period from the third to the tenth revolution. In the case of the square rotor ($N_{mag} = 4$), the friction force for the single-layer/double-layer stator is 0.013 H and 0.0021 H, respectively. In the case of the octagonal rotor ($N_{mag} = 8$), the friction force for the single-layer/double-layer stator is 2.01×10^{-6} H and 1.25×10^{-6} H, respectively. When $N_{mag} = 16$, the friction force for the single-layer/double-layer stator is 1.5×10^{-7} H and 8.1×10^{-8} H, respectively.

The typical distribution of the superconducting current density in the stator and the distribution of the square rotor magnetic field are presented in Fig. 5. The superconducting current lines are at the top of the figure, and the lines of the rotor magnetic field levels are at the bottom of the figure. A fragment of the stator

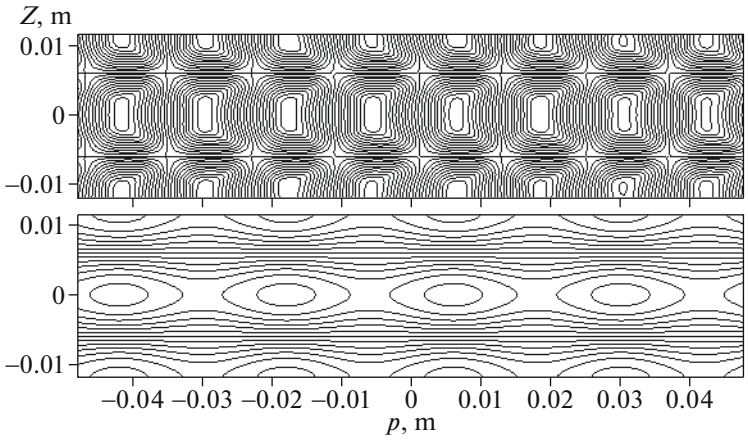

Fig. 5. Lines of superconducting currents (top of the figure) and lines of levels of the square rotor magnetic field component that is normal to the surface of the stator (bottom of the figure). The current line in the upper figure corresponds to the current value of 5 A. The line in the lower figure corresponds to the magnetic field induction of 0.02 T.

with the width of $2d_Z$ is presented in this figure (the central tape is surrounded by halves of neighboring tapes of the stator from above and from below). The picture is regularly displaced along the p axis with the turn of the rotor.

In order to obtain a qualitative interpretation of the friction force dependence on the number of magnets of the rotor and HTS tape coils of the stator, it is convenient to represent the stator as a system of interconnected magnetic pumps. We present each cell of the calculation grid $h \times h$ in size on the stator as an elementary magnetic pump. If the rotation frequency of the rotor is denoted as ω, the pumping frequency of each pump by the external variable magnetic field is $\omega \cdot N_{mag}$ (the phase of oscillations of the field is different for cells with different p coordinates). The magnetic moment of a cell induced by the external field is $g \cdot \mathbf{n}_\rho \cdot h^2$. In this expression, $\mathbf{n}_\rho$ is the unit vector normal to the surface of the stator, and g is the magnetic moment density related to the stator surface current density $\mathbf{j}(p, Z)$ by the relation $\mathbf{j}(p, Z) = \nabla \times (g \cdot \mathbf{n}_\rho)$ (see [5] and references thereof). In Fig. 6, the dependence of the magnetic moment density of the cell with the coordinates $p = 0$ and $Z = 0$ on the rotor induction density at this point is presented. The top curve represents the single-layer stator, and the bottom curve shows the double-layer HTS stator. The dependences are displayed for one revolution of the rotor after the transients are completed. The values of the magnetic field induction at this point change from the minimum $B_{\min} = 0.095$ T to the maximum $B_{\max} = 0.128$ T.

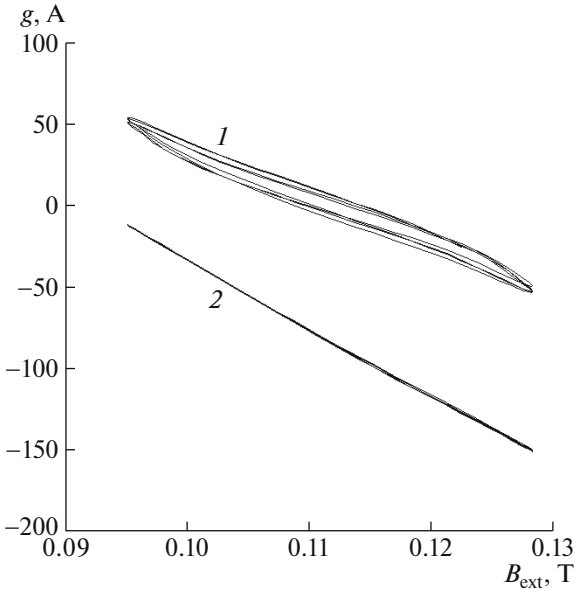

Fig. 6. Dependences of the magnetic moment density at the point with coordinates $p = 0$ and $Z = 0$ on the magnetic field induction per one revolution of the rotor for the cases of (*1*) single-layer stator and (*2*) double-layer stator. Arrows indicate the direction of traversal of the hysteresis curve at the rotor rotation.

Over the segment of the curve corresponding to the increase in the field induction from the minimum $B_{\min}$ to the maximum $B_{\max}$, the EMF of the varying field induces currents that decrease the magnetic moment density (the induced magnetic field is opposite to the inducing field). Consequently, the magnetic moment attains its minimum at the peak of the magnetic field. This "shielding" process is limited by the finite value of the critical current (otherwise, the "shielding" would be total over the whole stator). At the initial stage of the magnetic field decrease from the peak value, the EMF changes sign, and the current density becomes less than critical at this point. In the course of further decrease in the field, the current density passes zero and attains its critical value again. The amplitude of variation of the square rotor magnetic

field induction on the stator surface attains 14.8% of the average level. Firstly, this change is sufficient to alter the sign of the magnetic moment of a unit cell of the single-layer stator (see Fig. 6, top curve), while the magnetic field sign is constant. Secondly, the smallness of the critical current while the field undergoes this change implies the radical magnetic reversal of the stator, which provides a wide hysteresis loop (and consequently induces dissipation of energy and a significant friction force). The twofold increase in the critical current density of the double-layer stator blocks the process of magnetic reversal (see Fig. 6, bottom curve). The area of the hysteresis loop sharply decreases, and consequently, the friction force decreases. A considerable decrease in the friction force with the increase in the number of magnets has a similar explanation. The magnetic field amplitude variations by 1.3% and 0.2% for $N_{mag} = 8$ and 16, respectively, are not sufficient for the magnetic reversal of even a single-layer stator.

CONCLUSIONS

The calculations have shown that the magnetic friction force and the consequent energy losses do not hinder the creation of a combined bearing with a rotor composed of more than eight magnets and a stator consisting of a few short-circuit layers of the second-generation HTS tape. The experimental verification of this conclusion and the analysis of influence of other parameters of the bearing (eccentric arrangement and tilt of the rotor axis in relation to the stator axis, defects of the HTS tape of the stator, etc.), which can critically worsen its characteristics, will be carried out separately.

Note that the considered configuration of a magnetic rotor and a superconducting stator made of the HTS tape has a key advantage in comparison with the 3D HTS tape bearings because it allows a practically unlimited scaling of the device.

FUNDING

This study was supported by the Russian Science Foundation, project no. 17-19-01527.

CONFLICT OF INTEREST

The authors declare that they have no conflicts of interest.

REFERENCES

1. Y. Miyazaki, K. Mizuno, and T. Yamashita, Cryogenics **80**, 234 (2016).
2. W. Liu, G. Ma. Yang, T. Quéval, C. Ye. Gong, and Z. Li, Supercond. Sci. Technol. **31**, 015013 (2018).
3. M. V. Kozintseva, A. M. Bishaev, A. A. Bush, M. B. Gavrikov, K. E. Kamentsev, N. A. Nizhel'skii, V. V. Savel'ev, and A. S. Sigov, Tech. Phys. **62**, 890 (2017).
4. I. A. Rudnev and A. I. Podlivaev, IEEE Trans. Appl. Supercond. **26**, 8200104 (2016).
5. Ch. Jooss, J. Albrecht, H. Kuhn, S. Leonhardt, and H. Kronmuller, Rep. Prog. Phys. **65**, 651 (2002).
6. V. R. Romanovskii, Tech. Phys. **62**, 58 (2017).
7. V. R. Romanovskii, Tech. Phys. **62**, 553 (2017).
8. D. F. Alferov, M. R. Akhmetgareev, D. V. Evsin, I. F. Voloshin, A. V. Kalinov, L. M. Fisher, and E. V. Tskhai, Tech. Phys. **63**, 26 (2018).
9. L. D. Landau and E. M. Lifshitz, *Course of Theoretical Physics,* Vol. 2: *The Classical Theory of Fields* (Nauka, Moscow, 1988; Pergamon, Oxford, 1975).
10. B. A. Bazarov, V. F. Ezhov, N. A. Kovrizhnykh, V. L. Ryabov, A. Z. Andreev, A. G. Glushkov, V. A. Knyaz'kov, and G. B. Krygin, Tech. Phys. Lett. **42**, 663 (2016).
11. A. I. Podlivaev, S. V. Pokrovskii, I. V. Anishchenko, and I. A. Rudnev, Tech. Phys. Lett. **43**, 1136 (2017).
12. A. I. Podlivaev, I. A. Rudnev, and N. P. Shabanova, Bull. Lebedev Phys. Inst. **41**, 351 (2014).
13. C. P. Bean, Phys. Rev. Lett. **8**, 250 (1962); Rev. Mod. Phys. **36**, 31 (1964).
14. A. I. Podlivaev and I. A. Rudnev, Supercond. Sci. Technol. **30**, 035021 (2017).

Translated by N. Semenova